Equivalent Circuit Theory Assisted Deep Learning for Accelerated Generative Design of Metasurfaces

Wei, Zhaohui; Zhou, Zhao; Wang, Peng; Ren, Jian; Yin, Yingzeng; Pedersen, Gert Frølund; Shen, Ming

Published in:
IEEE Transactions on Antennas and Propagation

DOI (link to publication from Publisher):
10.1109/TAP.2022.3152592

Publication date:
2022

Document Version
Accepted author manuscript, peer reviewed version

Equivalent Circuit Theory-Assisted Deep Learning for Accelerated Generative Design of Metasurfaces

Zhaohui Wei, Zhao Zhou, Peng Wang, Jian Ren, *Member, IEEE,* Yingzeng Yin, *Member, IEEE,* Gert Frølund Pedersen, *Senior Member, IEEE,* and Ming Shen, *Senior Member, IEEE*

***Abstract*—In this paper, we propose an equivalent circuit theory-assisted deep learning approach to accelerate the design of metasurfaces. By combining the filter equivalent circuit theory and a sophisticated deep learning model, designers can achieve efficient metasurface designs. Compared with most existing metasurface generative design methods that rely on arbitrarily generated training data set (TDS), the proposed method can adaptively produce highly relevant and low-noise training samples under the guidance of filter equivalent circuit theory, resulting in a significantly narrowed target solution space and improved model training efficiency. Furthermore, we select the variational autoencoder (VAE) as a generative model, which can compress the raw training samples into a lower-dimensional latent space where optimization methods, such as genetic algorithm, can be more efficiently executed to find the optimal design than a brute-force search. To verify the effectiveness of the proposed method, we apply it in the creation of three examples of frequency selective surfaces (FSS), presenting wide-band, dual-band, and band-stop responses. Experimental results show that the proposed method can realize much faster and more stable convergence than deep learning design methods without domain knowledge.**

***Index Terms*—FSS, inverse design, generative design, variational autoencoder.**

I. Introduction

METASURFACES, as artificially periodic structures, are composed of many sub-wavelength uniform or non-uniform unit cells [1]. Owing to the extraordinary capability to manipulate the amplitudes, phases and polarization of electromagnetic (EM) waves, metasurfaces have been widely used for various applications such as spectrum filtering [2], polarization conversion [3], [4], vortex beam generation [5] and amplitude/phase modulation [6]. Traditionally, the design of metasurfaces mainly relies on engaging experienced engineers with a large number of iterative optimizations. To obtain a satisfactory design, time-consuming full-wave EM simulations are mandatory using traditional methods, which leads to a heavy computational burden. Furthermore, large scale complex metasurfaces, such as software-defined metasurfaces (SDMs) [7–9] and reconfigurable intelligent surfaces (RIS) [10–12], are playing an increasingly important role in the emerging beyond fifth/sixth-generation wireless communication systems. Design methods heavily relying on experience and EM simulations can no longer meet the expected design efficiency.

In recent years, machine learning (ML) based methods have attracted significant attention to accelerate device design. Thanks to the capability of learning from massive data and the increasing computing power provided by advanced GPUs, artificial neural network (ANN) has shown great promise for the modeling and design of microwave components, such as amplifiers [13], transistors [14], and antennas [15–17]. Existing machine learning-based design methods can be categorized into three groups: forward, inverse, and generative design. For forward designs, geometrical parameters of metasurface structures and their corresponding EM properties calculated by EM simulation tools are provided as features and labels, respectively. By using multilayered neural networks with nonlinear activation functions, such as deep neural networks (DNNs) [18], and convolutional neural networks (CNNs) [19], it is possible to uncover the hidden relationships between the features and the labels. However, the forward predicting networks cannot automatically converge toward the optimal solution. Thus, the trained neural network is repetitively called by an optimization algorithm to find the desired solution, typically with numerous iterations.

Apart from the forward design methods, many inverse design approaches [20–29] have been proposed and investigated. Contrary to the forward designs, EM responses of metasurface structures are set as the input while their corresponding geometrical parameters are the output of the neural network. Once the inverse DNN is trained, geometrical parameters can be obtained directly given the target EM responses. Various metasurface designs, such as single-layer metasurfaces [20], [21], multi-layer metasurfaces [22], dual-polarized metasurfaces [23] and coding programmable metasurfaces [24], [25], have been reported demonstrating the feasibility of the inverse design methods. Compared to the forward design methods, the inverse neural networks provide a higher design efficiency.

Generative neural network [30–32] is another powerful machine learning technique for metasurface designs. Two main generative models, generative adversarial network (GAN) [33] and VAE [34], are usually utilized to create metasurface structures. In Ref. [33], by employing three deep convolutional networks, a generator, a discriminator, and a predictor, the well-trained GAN can generate similar samples to the ones in the TDS and achieve a fast optimization. In Ref. [34], the VAE that consists of an encoder and a decoder converted

Manuscript received *** **, ****; revised *** **, ****. This work was sponsored by China Scholarship Council.

Zhaohui Wei, Zhao Zhou, Peng Wang, Gert Frølund Pedersen, and Ming Shen are with the Department of the Electronic Systems, Aalborg University, 9220 Aalborg, Denmark (e-mail: gfp@es.aau.dk; mish@es.aau.dk).

Jian Ren, and Yingzeng Yin are with the National Key Laboratory of Antennas and Microwave Technology, Xidian University, Xi'an 710071, China.

Color versions of one or more of the figures in this communication are available online at https://ieeexplore.ieee.org.

Digital Object Identifier:

high-dimensional original data to a low-dimensional latent space where particle swarm optimization (PSO) was efficiently performed to find the optimum solution.

The design methods for metasurfaces mentioned above have shown the promising potential of machine learning to enhance design efficiency mainly through constantly improving machine learning models. It is worth noting that apart from the learning models, the TDS is also a crucial factor that can influence design efficiency. But how to generate a high-quality TDS is not a trivial task.

To tackle this challenge, we propose a metasurface design technique by incorporating electromagnetic domain knowledge and generative machine learning. According to different design targets, the most relevant training samples can be identified guided by the filter equivalent circuit theory. Compared to most existing metasurface TDS generation techniques selecting arbitrarily from a mixed structure pool, the proposed method can take full advantage of prior knowledge from existing design theory and experience, which lays a solid foundation for the subsequent model training and optimization. The VAE is selected as a generative model, which can convert the raw high-dimensional data to a low-dimensional latent space where optimization methods can be implemented to search for the best solution, greatly improving the design efficiency.

The proposed technique is mainly aimed at the use case where there is a stringent requirement on the short design cycle and high performance of metasurfaces. Compared to the traditional equivalent circuit design methods that require solid theory and extensive experience, potential users of the proposed approach only need basic knowledge about metasurfaces to achieve a high-quality TDS generation, which significantly reduces the design difficulty. After completing the training, the proposed method is a fully automated design process that can efficiently search for the desired solution without intervention from the designer once the design target is given. Therefore, it is a promising auxiliary design approach for metasurface designs. The methodology of high-quality TDS generation is also suitable for other fields to improve the training efficiency of neural networks.

This paper is organized as follows. The problem formulation is presented in Section II. The proposed approach, which consists of TDS generation, VAE modeling, and optimization, is introduced in Section III. Section IV shows three application examples. The discussion and conclusion are given in Section V and VI, respectively.

II. Problem Formulation

TDSs and learning models are the two most crucial building blocks for machine learning-assisted designs. However, in existing metasurface designs, the design efficiency is improved mainly through constantly optimizing learning models. Generating the most relevant TDS based on EM domain knowledge is rarely investigated. Therefore, in the process of TDS generation, a large quantity of invalid data are often included due to the lack of domain knowledge, which will deteriorate learning model performance.

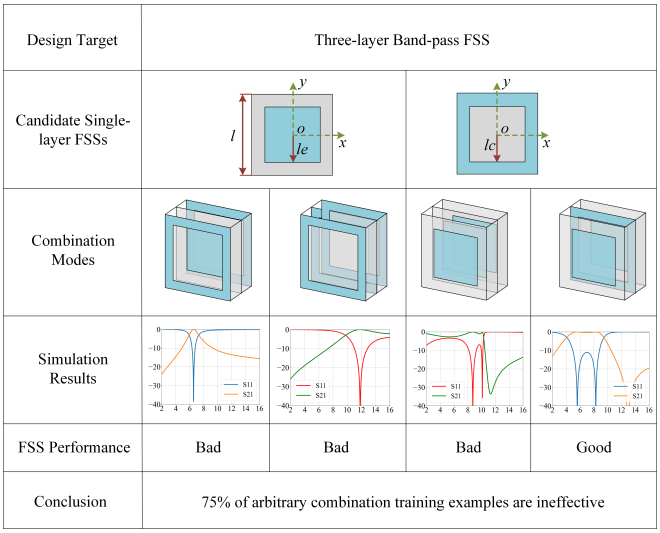

Fig. 1. An example of conventional multi-layer FSS TDS generation method using random combinations of arbitrary FSS candidate elements. (Element dimensions in the example: l = 12 mm, le = 4 mm, lc = 5 mm)

The existing multi-layer FSS TDS generation method consists of two steps [34]: prepare many different kinds and sizes of candidate single-layer FSSs and then randomly select the single-layer FSSs to form the multi-layer FSSs in an arbitrary combination manner. The stochastic selection and combination approach produce a low-quality TDS polluted by quantities of low-relevant, even invalid data. To outline this problem, a three-layer band-pass FSS TDS generation is demonstrated, as shown in Fig. 1. For the ease of problem formulation, only two candidate single-layer FSSs are provided for forming the three-layer FSSs, and the top and bottom layers of the formed three-layer FSSs are identical. Based on the stochastic selection and combination method, four types of FSSs training examples can be constituted, and the corresponding simulated S-parameters are depicted in Fig. 1. The results show that only one out of the four cases can achieve an excellent band-pass characteristic, which the equivalent circuit theory can explain in the following subsection. For the given simple case, 75% of the stochastic training examples are ineffective, not to mention the more complicated issues that provide a large number of candidate single-layer FSSs and thousands of combination modes. Therefore, the conventional multi-layer FSS generation method that forms the training examples in the stochastic selection and the arbitrary combination will remarkably reduce the training efficiency and deteriorate model performance.

III. The Proposed Approach

A. Generative Design Flow

To better understand the proposed design approach, we take frequency selective surfaces (FSSs) as examples for demonstration, and the flowchart of the generative design is given in Fig. 2. As shown in Fig. 2, the design procedure mainly consists of three parts: TDS generation, generative model construction, and model optimization. Different from the existing metasurface design methods that use a single complex machine learning (ML) model and mix a large number of metasurface

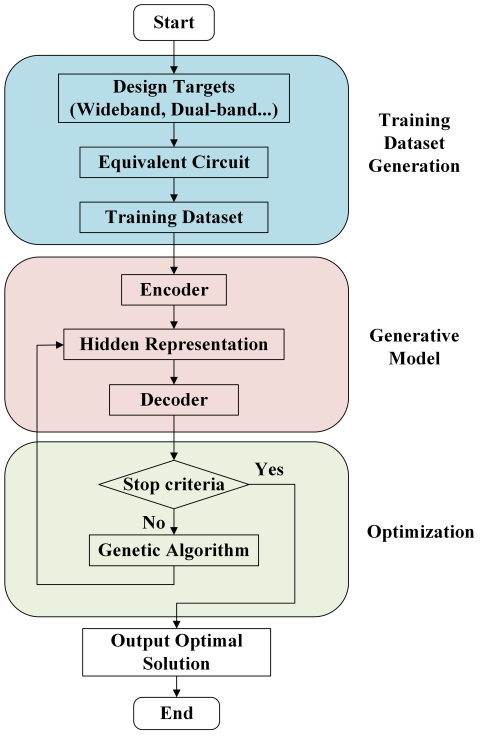

Fig. 2. Flowchart of the generative design approach for metasurfaces.

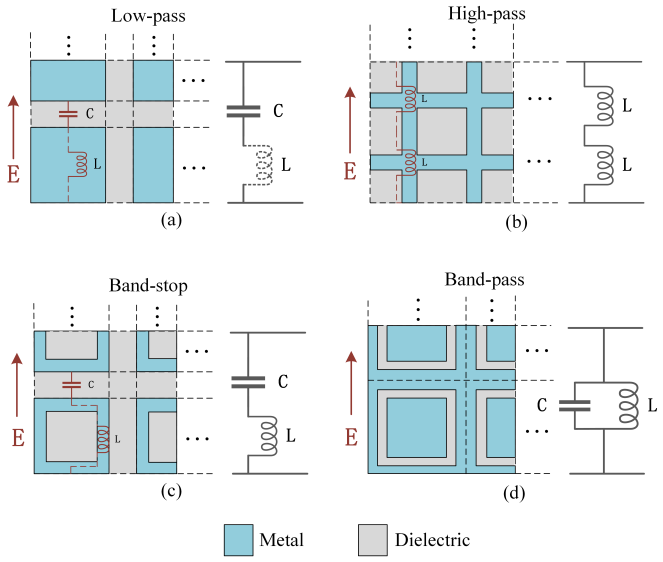

Fig. 3. Basic structures and their corresponding equivalent circuits.

unit patterns with varying EM characteristics together as one data set for training, the proposed method employs multiple simple ML models combined with small quantities of TDS with specific EM properties, leading to a higher optimization efficiency. According to different frequency responses, the design targets are divided into different categories, such as wide band-pass FSS, dual band-pass FSS, and stop-band FSS. Thanks to the guidance of the corresponding filter equivalent circuit, designers can determine the number of layers and candidate unit patterns of each layer. Compared to training samples by randomly selecting from a hybrid structure pool, the ones produced by the proposed method are of higher relevance and quality. A VAE as a generative model and genetic algorithm is utilized to create new FSS structures and accelerate the optimization to achieve data compression and improve design efficiency. The details will be demonstrated in the following subsections.

B. Equivalent Circuit Theory-Assisted TDS Generation

The equivalent circuit theory is used to generate the TDS efficiently. Firstly, based on the design target, a lumped element filter prototype that meets the EM properties is given as an equivalent circuit for the FSS structure. These lumped elements are replaced with corresponding FSS structures according to the relationship between the FSS unit patterns and their equivalent circuits.

To understand the relation between the equivalent circuits and FSS structures, two fundamental principles of FSS designs are given based on [35]. The patch type FSS (such as a ring element), whose equivalent circuit is a series resonant circuit, has a band-stop characteristic. In contrast, the slot type FSS (such as a hole element), equivalent to a parallel resonant circuit, shows a band-pass property. Another general principle is that the metal area of an FSS element is usually equivalent to inductance (L), which a two-parallel-wire model can explain; the gap creates a capacitance (C) effect, whose mechanism can be understood using a parallel plate capacitor model. According to the electrostatic principles, their values are given by:

$$L = \frac{l}{\pi} \ln(d_l/a) \tag{1}$$

$$C = \varepsilon_0 \varepsilon_r A/d_c \tag{2}$$

where ϵ_0, ϵ_r are two constants, A stands for the area of parallel plate capacitor, and d_c is the separation between parallel plate capacitor. l, d_l, a represent the length, distance, and radius of the two-parallel-wire, respectively.

The widely used FSSs structures can be grouped into four categories: low-pass, high-pass, band-pass, and band-stop FSS. We give one typical example of every kind of FSS, as shown in Fig. 3. In the case of Fig. 3(a), a wide patch element corresponds to a large area A of the parallel plate capacitor, a large radius a, and a small distance d_l of the two-parallel-wire. The formulas (1) and (2) show that the patch element has a low inductance value but a high capacitive value. In such a condition, the inductance can be negligible, and the capacitance will cut off high-frequency electromagnetic waves; therefore, the patch element shows a low-pass characteristic. In terms of Fig. 3(b), the long grid metal strips correspond to a considerable length l, a wide spacing d_l, and a small radius a of the two-parallel- wire; thus, it has a significant inductance value. Also, it corresponds to a wide separation d_c of the parallel plate capacitor, which means the capacitance value is minimal. In contrast to the inductance, the capacitance is negligible and should be ignored. Therefore, the inductance will cut off low-frequency electromagnetic waves, leading to

a high-pass property. Unlike the two former conditions, in the case of Fig. 3(c) and (d), we can see from the eq. (1) and (2) that neither the inductance nor the capacitance has an obvious advantage. Thus, the resonant circuits will cut off electromagnetic waves at the resonant frequency, resulting in a band-stop or band-pass performance. It is noted that the FSS elements given here are only with a single resonant frequency. The proposed method can also be suitable for the analysis of dual resonant (e.g., Jerusalem cross, frame-cross), multiple resonant (e.g., multiple square loops), and even more complex FSS elements whose equivalent circuits can be easily obtained [36], [37].

The process of TDS generation is depicted in Fig. 4. Each single-layer FSS comprises the metal meta-unit pattern represented by the blue region and the substrate denoted by the gray part. For multi-layer FSS designs, the training samples consist of multiple single-layer FSSs. Different from the existing multi-layer FSS generation method that randomly selects single-layer FSSs from one mixed training sample pool to form a multi-layer FSS, the proposed method classifies the training sample pool into the four basic categories as shown in Fig. 3 based on the transformation between FSS structures and equivalent circuits. Next, to determine the candidate FSS of each layer, an equivalent filter circuit will be provided according to the design requirement. For example, a band-pass filter equivalent circuit is proposed in Fig. 4. We can see from the equivalent filter circuit that the first and third elements are identical capacitors while the second element is an inductor. Therefore, the top and bottom layers are identical structures, and their candidates should be selected from the capacitive FSS category. Meanwhile, the candidates of the middle layer should be chosen from the inductive FSS category. With the assistance of basic FSS candidate categories and the equivalent filter circuits, higher-quality TDSs can be efficiently produced. In our work, each generated training sample is composed of $28 \times 28 \times 3$ pixels described by a $28 \times 28 \times 3$ matrix. An F4B dielectric slab with a dielectric constant of 2.65 and a loss tangle of 0.009 is utilized as the dielectric spacer.

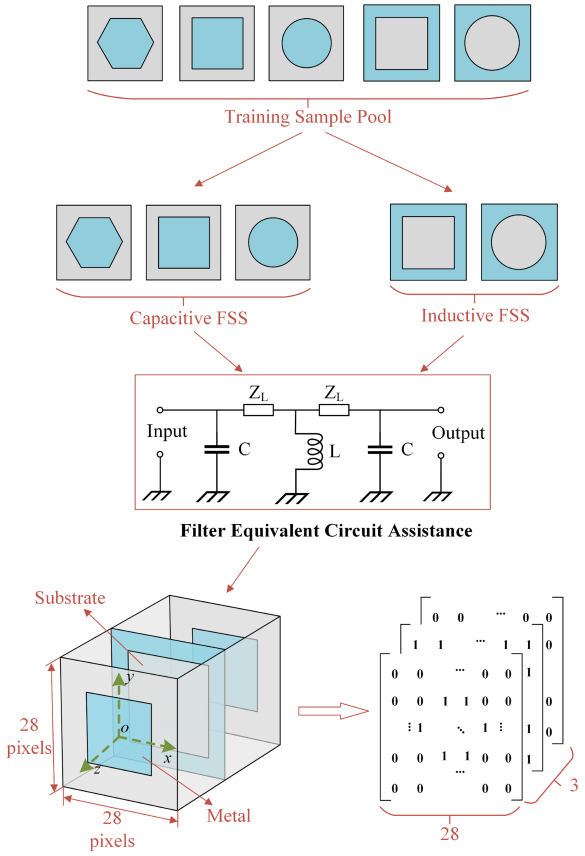

Fig. 4. FSS TDS generation based on the equivalent circuit theory.

TABLE I
PARAMETERS OF ENCODER NEURAL NETWORK

No. of layers	First	Second	Final
Input channels	1	16	32
Output channels	16	32	10
Kernel size	4	4	4
Stride	2	2	2
Batch normalization	Yes	Yes	No
Activation function	ReLU	ReLU	No

C. VAE Model

Fig. 5(a) shows a scheme for the VAE model. As shown in Fig. 5(a), a VAE is a neural network architecture composed of an encoder and a decoder that is trained to minimize the reconstruction error between the encoded-decoded data and the initial data. Compared with a conventional autoencoder, which maps each data to a single point in the latent space (z-space), the encoder of VAE outputs the mean and covariance matrices of a multivariate normal distribution where all of the dimensions are independent. In such conditions, some regularity has been introduced to the latent space. We can generate new data by sampling a point from that distribution and passing it to the following decoder. Once the VAE is well trained, its decoder can be used as a generative model.

The encoder and decoder neural network schemes are shown in Fig. 5(b) and Fig. 5(c) in detail. Through using three convolutional operations represented by black dashed lines in Fig. 5(b), each high-dimensional input pattern is compressed to a lower-dimensional tensor. We can also find from Fig. 5(b) that the batch normalization and ReLU activation function, represented by pink and purple planes, are removed in the last convolutional operation. The decoder is the inverse process of the encoder. Four transpose convolutional operations (ConvTranspose2d), as shown in black dashed lines in Fig. 5(c), are utilized to up-sample and generate new patterns. It is worth mentioning that the batch normalization is removed, and the ReLU activation function is replaced by Sigmoid after the last transpose convolutional operation. Table I shows the detailed parameters of the encoder, and that of the decoder are listed in Table II.

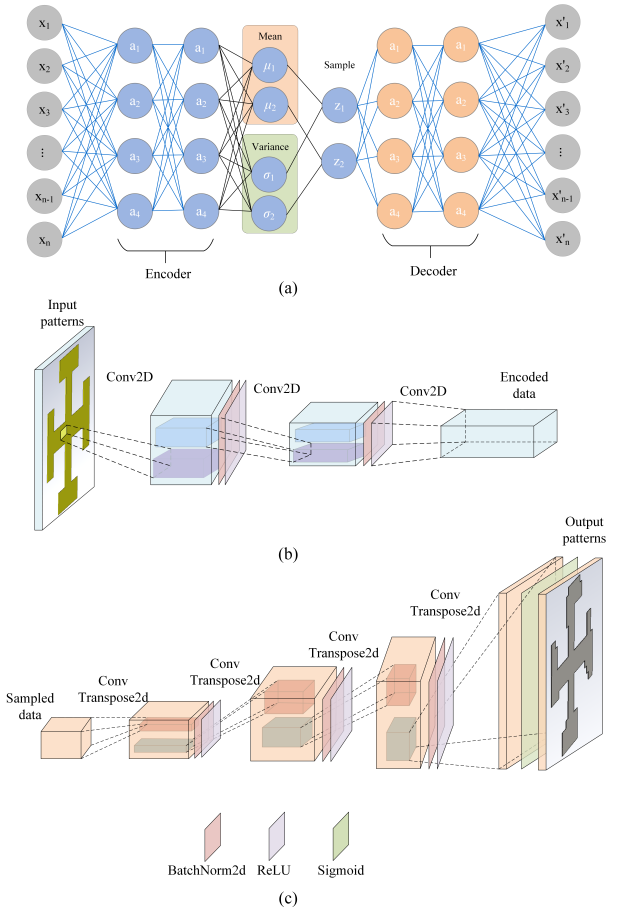

Fig. 5. (a) The entire variational autoencoder architecture. (b) The detailed encoder architecture. (c) The detailed decoder architecture.

TABLE II
PARAMETERS OF DECODER NEURAL NETWORK

No. of layers	First	Second	Third	Final
Input channels	5	256	128	64
Output channels	256	128	64	1
Kernel size	3	4	3	4
Stride	2	1	2	2
Batch normalization	Yes	Yes	Yes	No
Activation function	ReLU	ReLU	ReLU	Sigmoid

D. Optimization

Fig. 6 illustrates the flowchart of the genetic algorithm for latent representation optimization. As shown, the population is initialized by encoding the FSS structures into latent representations, which are evolved in every iteration to search for the optimum solution in the latent space. The evolution process is composed of reproduction based on fitness [34], crossover and mutation. A new population can be generated and applied for the next iteration through these operations until the desired solution is found.

In order to evaluate the fitness of samples, an appropriate loss function is defined using minimum/maximum tolerable

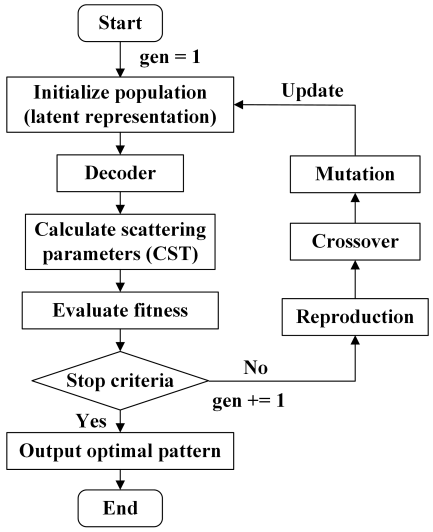

Fig. 6. Flowchart of genetic algorithm.

values over the frequency band of interest, which is similar to that in literature [34]. As shown in formula (3), the loss function L is composed of two terms: loss of reflection coefficient LS_{11} and loss of transmission coefficient LS_{21}. γ is ratio coefficient, which is used to adjust the loss function according to different design targets. In this paper, reflection coefficients of the FSS samples are mainly concerned, thus γ is set to 1. In formula (4) and (5), $\boldsymbol{S_{11}}$, $\boldsymbol{S_{21}}$ denote the reflection and transmission coefficients of FSS samples. $\boldsymbol{S_{min}}$, $\boldsymbol{S_{min}}'$ represent the reflection and transmission coefficient's lower masks of the desired FSS. $\boldsymbol{S_{max}}$, $\boldsymbol{S_{max}}'$ represent the reflection and transmission coefficient's upper masks of the desired FSS. Also, the boldface is denoted as row vector and $(*)^{\mathrm{T}}$ represents transpose operator.

$$L = \gamma \times LS_{11} + (1-\gamma) \times LS_{21} \tag{3}$$

$$\begin{aligned} LS_{11} = {} & (\boldsymbol{S_{11}} - \boldsymbol{S_{min}})(\boldsymbol{S_{11}} - \boldsymbol{S_{max}})^{\mathrm{T}} \\ & + \left|(\boldsymbol{S_{11}} - \boldsymbol{S_{min}})(\boldsymbol{S_{11}} - \boldsymbol{S_{max}})^{\mathrm{T}}\right| \end{aligned} \tag{4}$$

$$\begin{aligned} LS_{21} = {} & (\boldsymbol{S_{21}} - \boldsymbol{S_{min}}')(\boldsymbol{S_{21}} - \boldsymbol{S_{max}}')^{\mathrm{T}} \\ & + \left|(\boldsymbol{S_{21}} - \boldsymbol{S_{min}}')(\boldsymbol{S_{21}} - \boldsymbol{S_{max}}')^{\mathrm{T}}\right| \end{aligned} \tag{5}$$

It can be found from these formulas that if $\boldsymbol{S_{11}}$/$\boldsymbol{S_{21}}$ is between the desired bounds indicated by $\boldsymbol{S_{min}}$/$\boldsymbol{S_{min}}'$ and $\boldsymbol{S_{max}}$/$\boldsymbol{S_{max}}'$, the L will becomes zero. Otherwise, it will be penalized based on the degree that the $\boldsymbol{S_{11}}$/$\boldsymbol{S_{21}}$ is out of the desired bounds.

IV. APPLICATION EXAMPLES

To verify the effectiveness and efficiency of the proposed method, we give three examples of FSS presenting wide-band, dual-band, and band-stop frequency responses. For simplicity, these examples are all three-layer FSS structures. The used F4B substrates have a dielectric constant of 2.65 and a loss tangle of 0.009.

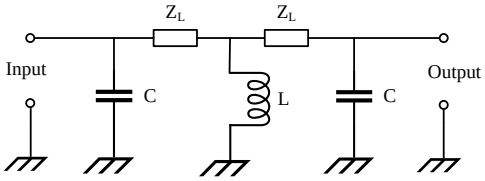

Fig. 7. Equivalent lumped element circuit of wide-band band-pass FSS.

A. Wide-band Band-pass FSS

In this case, the design target is given as follows: a wide-band band-pass FSS has a center frequency of 10.5 GHz, and the -10 dB relative bandwidth is 45%. According to the design requirement, a three-order filter prototype is selected, and the equivalent circuit is shown in Fig. 7. It can be seen that the designed FSS has three layers. The top and bottom layers are capacitive structures, and the middle layer is an inductive structure. Also, the candidate FSSs have identical top and bottom layers. Based on the relationship between FSS unit patterns and equivalent circuits, the solid patch replaces the capacitor while the inductor is substituted by its complementary structure. Three types of unit patterns for the top/bottom layer and the middle layer are given in Fig. 8. As shown in Fig. 8, the dielectric substrate has a length of 12 mm and a height of 2 mm. About 400 samples are used for training. Fig. 9 shows the optimal design of FSS. The green and red lines represent the minimum and maximum markers, respectively. The blue lines represent the scatter curves of FSS. We can see from the figures that the optimal FSS obtains a band-pass frequency response with a bandwidth of 47.6%. The optimal FSS structure is shown in Fig. 10(a). We can see that the top/bottom layers are quasi-circular unit patterns with a radius of around 3.5 mm. In contrast, the middle layer is a square slot structure with a length *ls* of around 5 mm. Fig. 10(b) compares the convergence curves when using the proposed TDS generated with domain knowledge for training and when applying the conventional approach without domain knowledge. The convergence of the proposed method is faster and more stable than the conventional approach without domain knowledge.

B. Dual-Band Band-pass FSS

In the design case of a dual-band band-pass FSS, the working bandwidth covers 8–10 GHz and 17–19 GHz. To satisfy the design requirement, an equivalent lumped element filter prototype is built and provided in Fig. 11. Three types of unit patterns are provided in Fig. 12, and the corresponding parameters are shown in Table III. The dielectric substrate has a length of 5 mm and a height of 1 mm. The optimal design of FSS is depicted in Fig. 13. Similar to the previous design case, the green and red lines represent the minimum and maximum markers, respectively. And the blue lines represent the scattering responses of the FSS. The desired result can be observed that the optimal FSS obtains a dual-band band-pass frequency response covering the frequency bands 8–10 GHz and 17–19 GHz. The optimal FSS structure is given in Fig. 14(a). It can be seen that the top/bottom layers are square

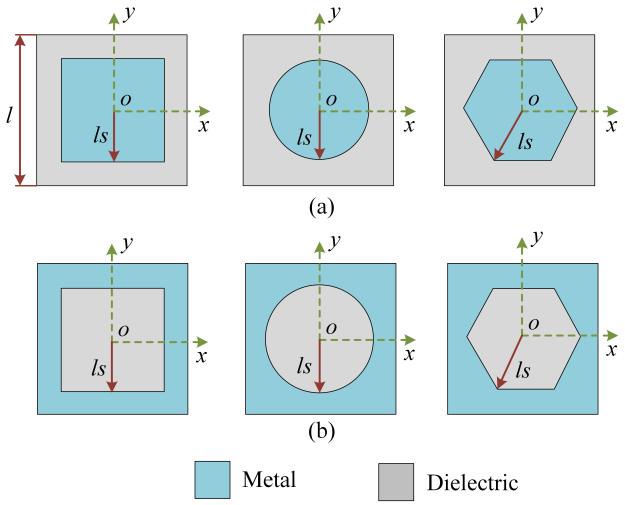

Fig. 8. Three types of unit patterns for (a) top/bottom layers (b) middle layer. (l = 12 mm, ls = 3 : 0.5 : 5.5 mm)

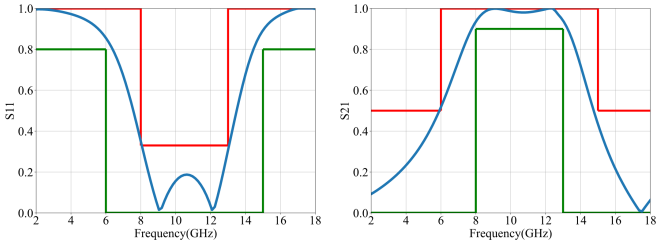

Fig. 9. Simulated S11 and S12 of the optimal wide-band band-pass FSS.

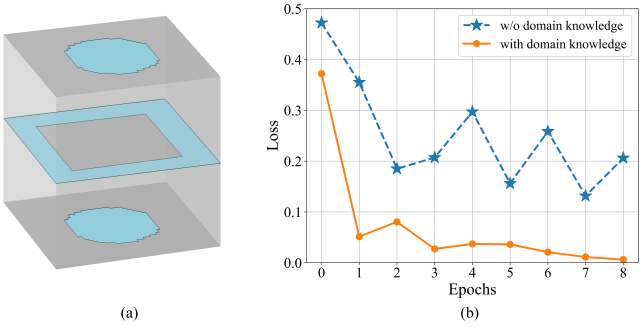

Fig. 10. (a) Optimal wide-band band-pass FSS structure. (b) Convergence comparison between the proposed method with domain knowledge (orange) and conventional approach without domain knowledge (blue).

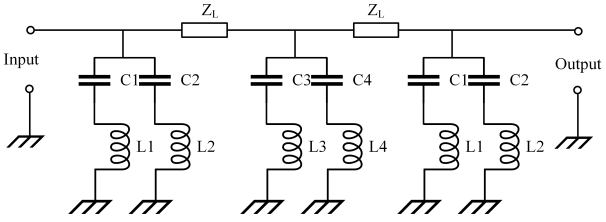

Fig. 11. Equivalent lumped element circuit of dual-band band-pass FSS.

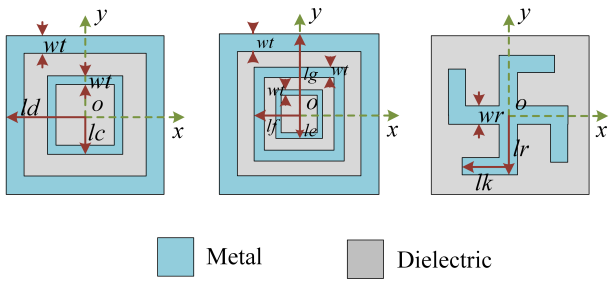

Fig. 12. Three types of candidate unit patterns for dual-band band-pass FSS.

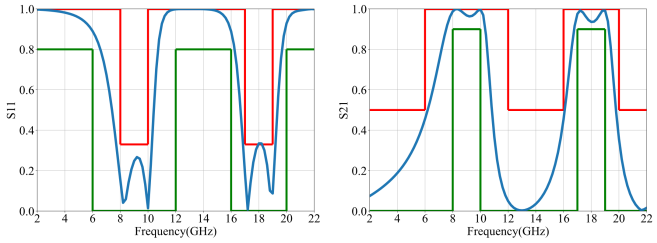

Fig. 13. Simulated S11 and S12 of the optimal dual-band band-pass FSS.

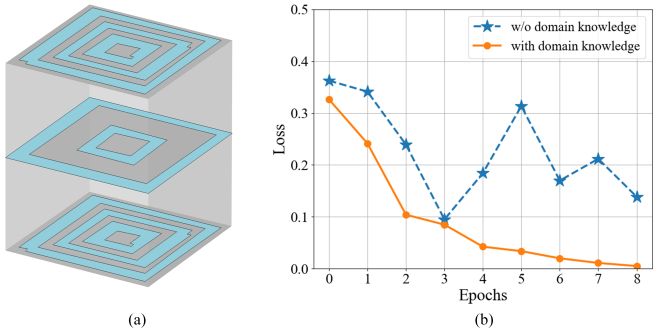

Fig. 14. (a) Optimal wide-band band-pass FSS structure. (b) Comparison between optimization convergence result with and without domain knowledge.

triple-ring unit patterns (le = 1.5, lf = 1.75, lg =2.5, wt = 0.5) while the middle layer is a square double-ring structure (lc = 2, ld = 2.5, wt = 0.5). Fig. 14(b) compares the convergence curves when using the proposed TDS generated with domain knowledge for training and when applying the conventional approach without domain knowledge. By comparison, the conventional method shows a slower convergence. Apart from the slower convergence, a relatively significant drop and rise of the training loss in the blue curve (conventional method without domain knowledge) at epochs 3 and 8 is observed. This shows that even if the conventional approach could hit some promising FSS design samples by luck, the benefit can be lost immediately due to the lack of guidance by mature equivalent circuit theory adopted in the proposed approach.

C. Wide-band Band-stop FSS

The third design example is a band-stop FSS. The target wide-band band-stop FSS should have a center frequency of 13 GHz, and the stop-band covers 8–18 GHz. According to this response requirement, an equivalent lumped element filter

TABLE III
PARAMETERS OF TDS

Parameters	Start(mm)	End(mm)	Step(mm)
lc	0.5	2	0.25
ld	1.5	2.5	0.25
wt	0.2	0.8	0.2
le	0.5	1.5	0.25
lf	1.75	2	0.25
lg	2.25	2.5	0.25
lk	1	4	0.5

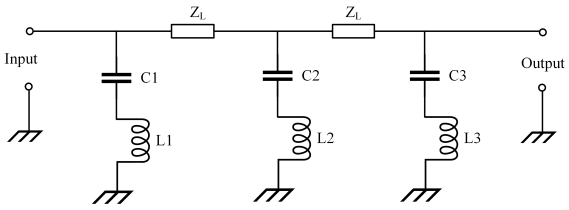

Fig. 15. Equivalent lumped element circuit of wide-band band-stop FSS.

prototype is provided in Fig. 15. Guided by the equivalent circuits, three types of unit patterns, as shown in Fig. 16, are utilized for constituting the TDS. The dielectric substrate has a length of 12 mm and a height of 2 mm. Fig. 17 shows the simulated results of the optimal FSS. We can see from the figures that the optimal FSS obtains a wide band-stop frequency response covering the frequency band 8–18 GHz, which fulfills the design requirement. The result of the optimal FSS structure is given in Fig. 18(a). It can be seen that the top/bottom layers are similar square-ring unit patterns (lr = 4.25, wr_top = 1.25, wr_bottom = 2.0) while the middle layer is a cross structure (lr = 4.0, wr = 2.0). As can be seen from Fig. 18(b), this design task is more challenging than the previous two design cases for the conventional ML-based approach. Without the guidance of FSS domain knowledge, conventional ML-based generative design methods need to go through all possible FSS element combinations of which a major group presents band-pass responses and not the relatively rare band-stop response that leads to inferior performance. Compared to the conventional method, our proposed method takes full advantage of the equivalent circuit to filter out the samples presenting band-pass responses, which results in higher design efficiency and faster convergence.

D. Comparison

The running time of the proposed method with and without domain knowledge are compared in Table IV. The CPU time of the two methods is calculated by the Pytorch ML framework on the platform of Python using a ThinkStation P920 Workstation computer. One can see that the proposed method with domain knowledge is four times faster than that without domain knowledge. Due to the guidance of equivalent circuits, massive invalid samples can be excluded from the solution space, which contributes to much less time for CST

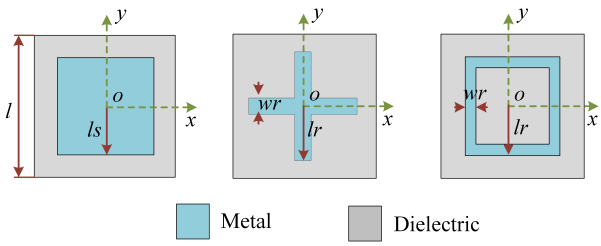

Fig. 16. Three types of candidate unit patterns for wide-band band-pass FSS. (l = 12 mm, ls = 3 : 0.25 : 5.5 mm, lr = 3 : 0.25 : 5.5 mm, wr = 1 : 0.25 : 2.5 mm)

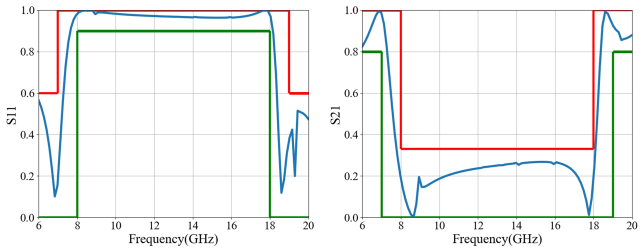

Fig. 17. Simulated S11 and S12 of the designed wide-band band-stop FSS.

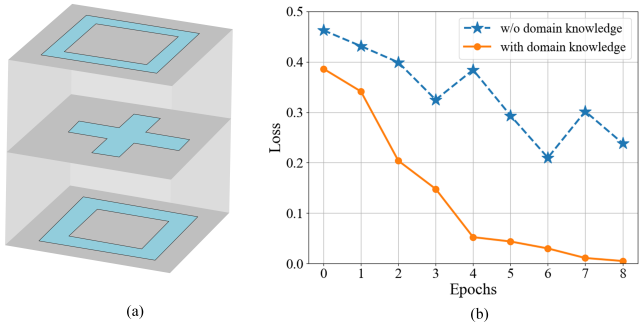

Fig. 18. (a) Optimal wide-band band-stop FSS structure. (b) Comparison between optimization convergence result with and without domain knowledge.

simulation. Also, a narrower solution space leads to a higher optimization efficiency. It is worth mentioning that although there is a time cost of introducing domain knowledge, it is negligible compared to the time spent in EM simulations.

V. Discussion

The proposed method reached the low loss threshold within a few epochs in all three design examples. At the same time, the conventional approach only obtained a higher loss with varied and unstable convergence performance. The reason can be easily found that the possibility of producing data with destructive EM properties significantly increased without the guidance of an equivalent circuit, which adds great complexity and difficulty to model training and leads to a low optimization efficiency.

Also, thanks to the continued efforts from FSS designers, the number of beneficial primary FSS signal samples increased. As a result, the design task will become even more challenging for conventional ML-based FSS design approaches. However, as the proposed method groups the primary FSS samples into a few categories based on their characteristics analyzed using mature equivalent circuit theory, the relevance of the new samples for the target designs is ensured. Therefore, the proposed method can achieve faster convergence and higher design efficiency. Promisingly, the proposed method can incorporate more pre-proven domain knowledge into the design and pave the way for more advanced design outcomes.

TABLE IV
Running Time of The Proposed Method With and Without Domain Knowledge

Overhead	With Domain Knowledge (h)	Without Domain Knowledge (h)
FSS Samples Generation	2	1
CST Simulation	20	110
Model Training	8	8
Optimization	0.5	2
Total	30.5	121

VI. Conclusion

In this paper, the TDS generation technique is investigated to accelerate the design of metasurfaces. We propose an equivalent circuit theory-assisted deep learning approach to achieve this goal. By combining the advantages of filter equivalent circuit theory that can roughly predict the FSS frequency response and deep learning that can uncover the hidden relations between input and output variables, the proposed method can significantly improve the design efficiency of FSS. Different from the conventional multi-layer FSS TDS generation that allows for arbitrary selection and combination, the proposed method can flexibly categorize the data into several groups based on equivalent circuit theory and adaptively form the multi-layer FSS, which reduces the probability of invalid data and lays a solid foundation for accelerating design, especially for large scale complex metasurfaces. The methodology of the TDS generation that combines domain knowledge and advanced deep learning techniques can not only serve for metasurface design but also provide a superior template for other machine learning-based applications.

References

[1] S. B. Glybovski, S. A. Tretyakov, P. A. Belov, Y. S. Kivshar, and C. R. Simovski, "Metasurfaces: From microwaves to visible," *Physics reports*, vol. 634, pp. 1–72, 2016.

[2] Z. Wang, C. Pang, Y. Li, and X. Wang, "A method for radiation pattern reconstruction of phased-array antenna," *IEEE Antennas and Wireless Propagation Letters*, vol. 19, no. 1, pp. 168–172, 2019.

[3] P. C. Wu, W. Zhu, Z. X. Shen, P. H. J. Chong, W. Ser, D. P. Tsai, and A.-Q. Liu, "Broadband wide-angle multifunctional polarization converter via liquid-metal-based metasurface," *Advanced Optical Materials*, vol. 5, no. 7, p. 1600938, 2017.

[4] B.-Q. Lin, J.-X. Guo, P. Chu, W.-J. Huo, Z. Xing, B.-G. Huang, and L. Wu, "Multiple-band linear-polarization conversion and circular polarization in reflection mode using a symmetric anisotropic metasurface," *Physical Review Applied*, vol. 9, no. 2, p. 024038, 2018.

[5] M. Mehmood, S. Mei, S. Hussain, K. Huang, S. Siew, L. Zhang, T. Zhang, X. Ling, H. Liu, J. Teng *et al.*, "Visible-frequency metasurface for structuring and spatially multiplexing optical vortices," *Advanced Materials*, vol. 28, no. 13, pp. 2533–2539, 2016.

[6] L. Liu, X. Zhang, M. Kenney, X. Su, N. Xu, C. Ouyang, Y. Shi, J. Han, W. Zhang, and S. Zhang, "Broadband metasurfaces with simultaneous control of phase and amplitude," *Advanced materials*, vol. 26, no. 29, pp. 5031–5036, 2014.

[7] S. Abadal, T.-J. Cui, T. Low, and J. Georgiou, "Programmable metamaterials for software-defined electromagnetic control: Circuits, systems, and architectures," *IEEE Journal on Emerging and Selected Topics in Circuits and Systems*, vol. 10, no. 1, pp. 6–19, 2020.

[8] A. Pitilakis, A. C. Tasolamprou, C. Liaskos, F. Liu, O. Tsilipakos, X. Wang, M. S. Mirmoosa, K. Kossifos, J. Georgiou, A. Pitsilides *et al.*, "Software-defined metasurface paradigm: Concept, challenges, prospects," in *2018 12th International Congress on Artificial Materials for Novel Wave Phenomena (Metamaterials)*. IEEE, 2018, pp. 483–485.

[9] A. C. Tasolamprou, M. S. Mirmoosa, O. Tsilipakos, A. Pitilakis, F. Liu, S. Abadal, A. Cabellos-Aparicio, E. Alarcón, C. Liaskos, N. V. Kantartzis *et al.*, "Intercell wireless communication in software-defined metasurfaces," in *2018 IEEE International Symposium on Circuits and Systems (ISCAS)*. IEEE, 2018, pp. 1–5.

[10] S. Zeng, H. Zhang, B. Di, Z. Han, and L. Song, "Reconfigurable intelligent surface (ris) assisted wireless coverage extension: Ris orientation and location optimization," *IEEE Communications Letters*, vol. 25, no. 1, pp. 269–273, 2020.

[11] J. Xu, Y. Liu, X. Mu, and O. A. Dobre, "Star-riss: Simultaneous transmitting and reflecting reconfigurable intelligent surfaces," *IEEE Communications Letters*, 2021.

[12] Z. Yigit, E. Basar, and I. Altunbas, "Low complexity adaptation for reconfigurable intelligent surface-based mimo systems," *IEEE Communications Letters*, vol. 24, no. 12, pp. 2946–2950, 2020.

[13] M. Isaksson, D. Wisell, and D. Ronnow, "Wide-band dynamic modeling of power amplifiers using radial-basis function neural networks," *IEEE Transactions on Microwave Theory and Techniques*, vol. 53, no. 11, pp. 3422–3428, 2005.

[14] B. Davis, C. White, M. A. Reece, M. E. Bayne, W. L. Thompson, N. L. Richardson, and L. Walker, "Dynamically configurable phemt model using neural networks for cad," in *IEEE MTT-S International Microwave Symposium Digest, 2003*, vol. 1. IEEE, 2003, pp. 177–180.

[15] J. Tak, A. Kantemur, Y. Sharma, and H. Xin, "A 3-d-printed w-band slotted waveguide array antenna optimized using machine learning," *IEEE Antennas and Wireless Propagation Letters*, vol. 17, no. 11, pp. 2008–2012, 2018.

[16] S. Lebbar, Z. Guennoun, M. Drissi, and F. Riouch, "A compact and broadband microstrip antenna design using a geometrical-methodology-based artificial neural network," *IEEE Antennas and propagation Magazine*, vol. 48, no. 2, pp. 146–154, 2006.

[17] D. Kan, D. Spina, S. De Ridder, F. Grassi, H. Rogier, and D. V. Ginste, "A machine-learning-based epistemic modeling framework for textile antenna design," *IEEE Antennas and Wireless Propagation Letters*, vol. 18, no. 11, pp. 2292–2296, 2019.

[18] S. An, C. Fowler, B. Zheng, M. Y. Shalaginov, H. Tang, H. Li, L. Zhou, J. Ding, A. M. Agarwal, C. Rivero-Baleine *et al.*, "A deep learning approach for objective-driven all-dielectric metasurface design," *ACS Photonics*, vol. 6, no. 12, pp. 3196–3207, 2019.

[19] T. Yuze, L. Hai, and Z. Qinglin, "On the application of deep learning in modeling metasurface," in *2019 International Applied Computational Electromagnetics Society Symposium-China (ACES)*, vol. 1. IEEE, 2019, pp. 1–2.

[20] X. Shi, T. Qiu, J. Wang, X. Zhao, and S. Qu, "Metasurface inverse design using machine learning approaches," *Journal of Physics D: Applied Physics*, vol. 53, no. 27, p. 275105, 2020.

[21] T. Qiu, X. Shi, J. Wang, Y. Li, S. Qu, Q. Cheng, T. Cui, and S. Sui, "Deep learning: a rapid and efficient route to automatic metasurface design," *Advanced Science*, vol. 6, no. 12, p. 1900128, 2019.

[22] P. Naseri and S. V. Hum, "A machine learning-based approach to synthesize multilayer metasurfaces," in *2020 IEEE International Symposium on Antennas and Propagation and North American Radio Science Meeting*. IEEE, 2020, pp. 933–934.

[23] F. Ghorbani, J. Shabanpour, S. Beyraghi, H. Soleimani, H. Oraizi, and M. Soleimani, "A deep learning approach for inverse design of the metasurface for dual-polarized waves," *arXiv preprint arXiv:2105.08508*, 2021.

[24] T. Shan, X. Pan, M. Li, S. Xu, and F. Yang, "Coding programmable metasurfaces based on deep learning techniques," *IEEE Journal on Emerging and Selected Topics in Circuits and Systems*, vol. 10, no. 1, pp. 114–125, 2020.

[25] Q. Zhang, C. Liu, X. Wan, L. Zhang, S. Liu, Y. Yang, and T. J. Cui, "Machine-learning designs of anisotropic digital coding metasurfaces," *Advanced Theory and Simulations*, vol. 2, no. 2, p. 1800132, 2019.

[26] J. Hou, H. Lin, L. Chen, F. Deng, and Z. Fang, "Study on the choices of design parameters for inverse design of metasurface using deep leargning," in *2020 IEEE MTT-S International Conference on Numerical Electromagnetic and Multiphysics Modeling and Optimization (NEMO)*. IEEE, 2020, pp. 1–4.

[27] L.-Y. Xiao, F.-L. Jin, B.-Z. Wang, Q. H. Liu, and W. Shao, "Efficient inverse extreme learning machine for parametric design of metasurfaces," *IEEE Antennas and Wireless Propagation Letters*, vol. 19, no. 6, pp. 992–996, 2020.

[28] L. Yuan, X.-S. Yang, C. Wang, and B.-Z. Wang, "Inverse design of metasurface using combined neural network and transfer function," in *2020 IEEE International Symposium on Antennas and Propagation and North American Radio Science Meeting*. IEEE, 2020, pp. 2027–2028.

[29] L. Yuan, L. Wang, X.-S. Yang, H. Huang, and B.-Z. Wang, "An efficient artificial neural network model for inverse design of metasurfaces," *IEEE Antennas and Wireless Propagation Letters*, vol. 20, no. 6, pp. 1013–1017, 2021.

[30] S. An, B. Zheng, H. Tang, M. Y. Shalaginov, L. Zhou, H. Li, M. Kang, K. A. Richardson, T. Gu, J. Hu *et al.*, "Multifunctional metasurface design with a generative adversarial network," *Advanced Optical Materials*, vol. 9, no. 5, p. 2001433, 2021.

[31] F. Wen, J. Jiang, and J. A. Fan, "Progressive-growing of generative adversarial networks for metasurface optimization," *arXiv preprint arXiv:1911.13029*, 2019.

[32] Z. Liu, D. Zhu, S. P. Rodrigues, K.-T. Lee, and W. Cai, "Generative model for the inverse design of metasurfaces," *Nano letters*, vol. 18, no. 10, pp. 6570–6576, 2018.

[33] H. P. Wang, Y. B. Li, H. Li, S. Y. Dong, C. Liu, S. Jin, and T. J. Cui, "Deep learning designs of anisotropic metasurfaces in ultrawideband based on generative adversarial networks," *Advanced Intelligent Systems*, vol. 2, no. 9, p. 2000068, 2020.

[34] P. Naseri and S. V. Hum, "A generative machine learning-based approach for inverse design of multilayer metasurfaces," *IEEE Transactions on Antennas and Propagation*, 2021.

[35] B. A. Munk, *Frequency selective surfaces: theory and design*. John Wiley & Sons, 2005.

[36] K. Katoch, N. Jaglan, and S. D. Gupta, "A review on frequency selective surfaces and its applications," in *2019 International Conference on Signal Processing and Communication (ICSC)*. IEEE, 2019, pp. 75–81.

[37] F. Costa, A. Monorchio, and G. Manara, "Efficient analysis of frequency-selective surfaces by a simple equivalent-circuit model," *IEEE Antennas and Propagation Magazine*, vol. 54, no. 4, pp. 35–48, 2012.

Zhaohui Wei was born in Shandong, China. He received the B.Sc. and M.Eng. degrees in electronic engineering from Xidian University, Xi'an, China, in 2017 and 2020, respectively. He is currently pursuing a Ph.D. degree with the Antennas, Propagation and Millimeter-Wave Systems Section, Department of Electronic Systems, Aalborg University, Aalborg, Denmark. His research interests include filtering antenna, frequency selective surface, deep learning-based methods for the design and analysis of antenna systems.

Zhao Zhou was born in Shaanxi, China. He received the B.Sc. and M.Eng. degrees in electronic engineering from Xidian University, Xi'an, China, in 2017 and 2020, respectively. He is currently pursuing a Ph.D. degree with the Antennas, Propagation and Millimeter-Wave Systems Section, Department of Electronic Systems, Aalborg University, Aalborg, Denmark. His research interests include dual-polarized antenna, wide-band antenna, machine learning-based methods for the design and analysis of antenna systems.

Peng Wang was born in Anqing, Anhui Province, China. He received the B.Sc. and M.Eng. degrees in electronic engineering from Xidian University, Xi'an, China, in 2017 and 2020, respectively. He is currently pursuing a Ph.D. degree with the Antennas, Propagation, and Millimeterwave Systems (APMS) section, Department of Electronic Systems, Aalborg University, Aalborg, Denmark. His current research interests include metasurfaces, deep learning, and reconfigurable intelligent surfaces.

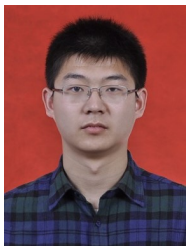

Jian Ren (Member'19) was born in Shandong, China. He received a B.Sc. degree and M.Eng. degree in electronic engineering from Xidian University, Xi'an, China, in 2012 and 2015, and a Ph.D. degree in electronic engineering from City University of Hong Kong in 2018. From March 2015 to August 2015, he was a Research Assistant with the City University of Hong Kong. In 2019, He joined the National Key Laboratory of Antennas and Microwave Technology, Xidian University, where he is now an Associate Professor. His current research interests include dielectric resonator antennas, millimeter-wave antennas, and metamaterials. He has authored or coauthored over 60 refereed journal articles. Dr. Ren received the Honorable Mention at the student best paper competition at the 2018 IEEE 7th Asia-Pacific Conference on Antennas and Propagation (APCAP). He has served as a reviewer for different peer-reviewed journals, including the IEEE Transactions on Antennas and Propagation, IEEE Transactions on Microwave Theory and Techniques, the IEEE Antennas and Wireless Propagation Letters, Applied Physics Letters, Optical Express, Optics Letters, and so on.

Yingzeng Yin received the B.S., M.S., and Ph.D. degrees in electromagnetic wave and microwave technology from Xidian University, Xi'an, China, in 1987, 1990, and 2002, respectively. From 1990 to 1992, he was a Research Assistant and an Instructor at the Institute of Antennas and Electromagnetic Scattering, Xidian University. He was an Associate Professor with the Department of Electromagnetic Engineering from 1992 to 1996 and has been a Professor since 2004. His current research interests include the design of microstrip antennas, feeds for parabolic reflectors, artificial magnetic conductors, phased array antennas, base-station antennas, and computer-aided design for antennas.

Gert Frølund Pedersen (SM'19) was born in 1965. He received the B.Sc. and E.E. (Hons.) degrees in electrical engineering from the College of Technology in Dublin, Dublin Institute of Technology, Dublin, Ireland, in 1991, and the M.Sc.E.E. and Ph.D. degrees from Aalborg University, Aalborg, Denmark, in 1993 and 2003, respectively. Since 1993, he has been with Aalborg University, a Full Professor heading the Antennas, Propagation, and Millimeter-wave Systems LAB with 25 researchers. He is also the Head of the Doctoral School on wireless communication with some 40 Ph.D. students enrolled. His research interests include radio communication for mobile terminals, especially small antennas, diversity systems, propagation, and biological effects. He has published more than 500 peer-reviewed papers, 6 books, 12 book chapters, and holds over 50 patents.

Ming Shen (Senior Member, IEEE) was born in Yuxi, China. He received the M.Sc. degree in electrical engineering from the University of Chinese Academy of Sciences (UCAS), Beijing, China, in 2005, and the Ph.D. degree in wireless communications, with the Spar Nord Annual Best Thesis nomination from Aalborg University, Denmark.

He is currently an Associate Professor in RF and mm-wave circuits and systems with the Department of Electronic Systems, Aalborg University. He has 20 years of experience in RF and millimeter-wave circuits and systems, including 12 years of experience in CMOS RF/mixed-signal IC design. He is also the Grant Holder and PI of two Danish national research projects and the Management Committee Member Substitute from Denmark in the EU COST Action IC1301 with the aim to gather the international efforts and address efficient wireless power transmission technologies. His current research interests include circuits and antennas for 5G and satellite communications, low power CMOS RF and millimeter-wave circuits and systems, circuits and systems for biomedical imaging, and artificial intelligence. He is a TPC Member of IEEE NORCAS. He serves as a Reviewer for the IEEE and Kluwer.